Materials Research. 2022; 25:e20210430
DOI: https://doi.org/10.1590/1980-5373-MR-2021-0430

Microstructural Analysis and Mechanical Behaviour of Copper CDA 101/AISI-SAE 1010 Dissimilar Metal Welds Processed by Friction Stir Welding

***K. Giridharan*[a]*, *P. Sevvel*[b], *B. Stalin*[c], *M. Ravichandran*[d], *P. Sureshkumar*[e]**

[a]*Easwari Engineering College, Department of Mechanical Engineering, 600089, Chennai, Tamil Nadu, India.*
[b]*S.A. Engineering College, Department of Mechanical Engineering, 600077, Chennai, Tamil Nadu, India.*
[c]*Anna University, Regional Campus Madurai, Department of Mechanical Engineering, 625019, Madurai, Tamil Nadu, India.*
[d]*K. Ramakrishnan College of Engineering, Department of Mechanical Engineering, 621112, Trichy, Tamil Nadu, India.*
[e]*Ramco Institute of Technology, Department of Mechanical Engineering, 626117, Rajapalayam, Tamil Nadu, India.*

Received: August 26, 2021; Revised: October 26, 2021; Accepted: December 3, 2021

In this work, low-carbon steel AISI-SAE grade 1010 with copper grade CDA 101 was joined by friction stir welding (FSW) using a tapered pin profiled tool. The rotational speed of the tool is 900 rpm, a traverse rate of 30 mm/min, and an axial force of 5 kN were used to produce the joints. The microstructural analysis and mechanical properties of the weld joints have been successfully examined. The optical microscopy, scanning electron microscopy, and X-ray diffraction (XRD) techniques were performed to examine the macropatterns and micropatterns of the welded joints. The tensile and hardness test was performed to evaluate the mechanical behaviours of the FSW joints. The fine ferrite grain features with uniform size were obtained in the microstructure of the nugget zone (stir zone). It is purely influenced by the alternating dynamic rearrangement (recrystallization) mechanism. High hardness was identified in the stir zone, even as the slightest stability was established in the heat-affected zone. The tensile investigation proposed that all the joints explored just lesser unbending nature than the parent material. The tensile strength of 181.5 MPa, the hardness of 144 VHN, and elongation of 14.03% were observed for the welded samples. The better properties for the weld joints were attained at 900 rpm spindle speed and tool traverse speed of 30 mm/min. The FSW is an attractive material joining process for both similar and dissimilar materials compared to other conventional types of joining processes, such as aerospace, marine engineering, shipbuilding, and industrial sector applications.

Keywords: *Copper, low-carbon steel, friction stir welding, mechanical properties, microstructure.*

1. Introduction

Effects of microstructure on hardness, microstructural characterization of dissimilar and similar metals of friction stir welding (FSW) joints and mechanical behaviours on low-carbon steel (LCS), stainless steel, aluminium alloy and magnesium alloy were investigated [1–5]. The grain size, grain and phase boundary characteristics, and local misorientation were studied through microstructural characterization by welding of different steel grades [6–7]. The dynamics of the weld melt pool were investigated in the laser welding process of a low-carbon/stainless steel joint [8]. Several studies have revealed that dissimilar weld configurations of Al to steel, Mg to steel, Al to Ti, Mg to Ti, Al to Cu, and Al to Mg offer enormous industrial prospective [9]. Furthermore, according to research studies, the industrial applicability of friction stir welding is increasing due to the rapid demand for high strength welded metal components in the automobile, aerospace, and structural sectors [10]. Many measures were taken in tool profile, tool material, tool design, and welding parameters in response to industrial requirements [11]. In addition, several research investigations used to conduct macro and microstructure studies in the heat-affected zone (HAZ) of weldments [12–13]. Many research have been reported on the formation of residual stresses in dissimilar metal welding, as well as diffusion and precipitation properties [13–15]. FSW process parameters and applications were discussed. The welded joints properties and their effects were analysed [16-17].

High-performance joining techniques and its properties were investigated in aluminium alloys. The developed joints were used in aircraft industries [18]. Joints with different composite materials and its applications have been discussed in aerospace applications [19]. The ageing procedures and its effect on microstructure were investigated in Al-Zn-Mg-Cu alloys [20]. FSW of aluminium was conducted without melting it in the weld nugget [21]. Thermomechanical-affected zone

*e-mail: girimech4305@gmail.com

(TMT) and rotational speed were studied in dissimilar joints AA7075 and AA2024 [22]. The magnesium and aluminium alloys have been joined through ultrasonic-based FSW [23]. Different friction welding zones of steel were exposed to metallographic examinations [24]. The impact of tool rotational speed and preheated specimen affects the microstructure of the welded joints [25]. The hardness and tensile strength in the stir zone of the welded nugget has been increased due to the development of fine grains [26]. High-level fatigue was found in the weld zone [27–28]. The microstructures and mechanical behaviours have been affected by the welding parameters [29]. Tensile and bend testing have been analysed in friction stir welding of 12% chromium alloy and LCS [30]. The better tensile properties were obtained during FSW of different steels. The metallographic changes have been recorded before and after the welding process [31]. The impacts of welding parameters on tensile behaviours and its microstructure were refined with a new austenite structure [32–33].

From the above-mentioned literature, the present study aims to investigate the microstructure and mechanical behaviours of friction stir-welded dissimilar LCS AISI/SAE grade 1010 with Copper grade CDA 101. The microstructural and mechanical behaviours of the welded joints have been investigated. The chemical compositions of the welding zone were analysed through energy dispersive analysis of X-rays (EDAX).

2. Materials Preparation and Methodology

The parent material used in this study is an LCS (AISI/SAE grade 1010) with Copper (CDA 101) alloys. The two dissimilar materials are machined for the size of 100 mm × 50 mm × 3 mm and used to prepare friction stir weld joints. The metal plates were prepared as per the required dimensions with the help of a power cutting machine and followed by a milling process to avoid sharp edges of the specimen. The parent materials are secured clamped in the weld position by using manual top clamps. The alloy combinations present in the parent materials are presented in Table 1. FSW setup is depicted in Figure 1(a). Figure 1(b) shows the schematic of the FSW operation. Tool material is an art form of the FSW process. The joint quality and wear of tool material is a significant consideration while selecting material for the FSW tool. The tool was fabricated using high carbon, high chromium material for this investigation. It has been already proven by several researchers that, tool rotational speed in the range of 800 rpm to 1200 rpm and welding speed of 20 mm/min to 40 mm/min were effective in fabricating superior quality FSW joints [12,17,25]. Based on these literature reviews, we have employed a constant tool rotational speed of 900 rpm and welding speed of 30 mm/min using the taper cylindrical shape tool as seen in Figure 2(a). The FSW tool is plunged and moved with high rigidly in the direction of the weld position as shown in Figure 2(b).

Table 1. Evaluation of base metal (BM) alloy composition (expressed in wt.%) of the copper and steel plate used at the present work.

Elements	Sn	Mn	Si	Mg	Al	S	Cr	Fe	P	Pb	Zn	Fe	Cu	-
Weight %	0.001	0.001	0.001	0.001	0.001	0.002	0.01	0.016	0.005	0.005	0.014	0.016	99.93%	-
Elements	Pb	Si	Cr	S	Mo	P	Ti	Cu	Ni	V	Al	W	C	Fe
Weight %	0.009	0.011	0.012	0.013	0.013	0.022	0.004	0.021	0.021	0.005	0.05	0.05	0.050	99.5%

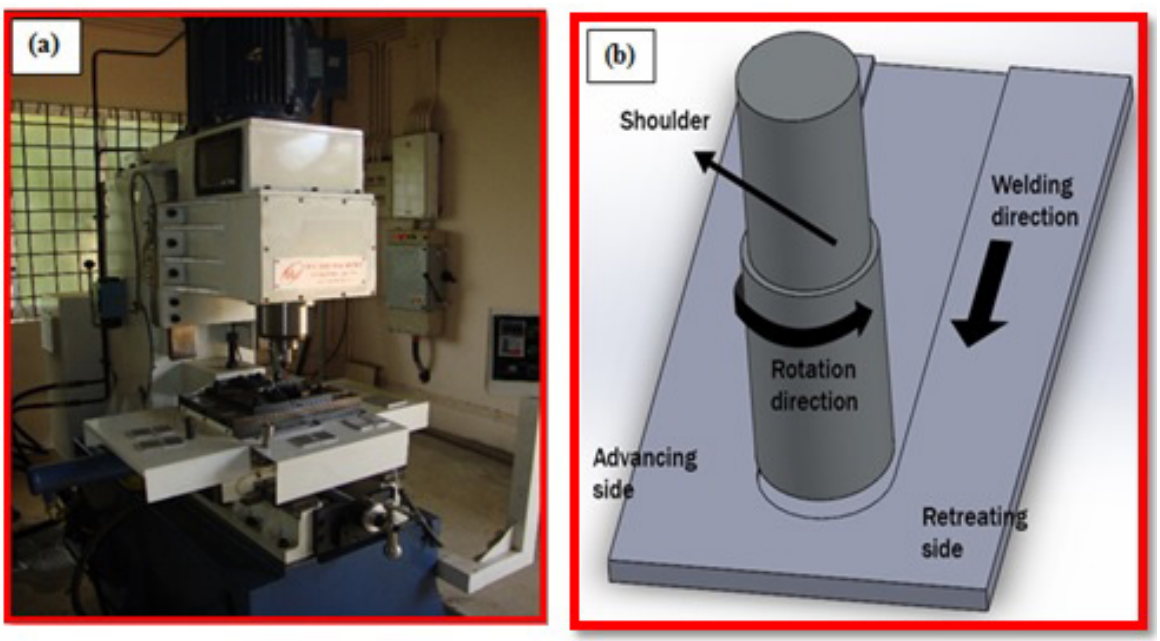

Figure 1. (a) A photographic view of FSW arrangement. (b) Schematic of FSW process.

The taper profiled FSW tool consists of shank diameter, shoulder diameter, tool pin length, and pin diameter. Cone-shaped pin having 3 mm shoulder diameter and 10° cylindrical, with an overall length of a 2.85 mm was used to carry out the joining process. Similarly, for all welding models, a constant dwell time of 5 s and a plunging depth of 0.2 mm were maintained. The dwell time was manually calculated using a digital stop watch. Before starting the welding process, the base materials of LCS AISI/SAE grade 1010 were positioned on the advancing side (AS) and copper CDA 101 plates were positioned on retreating side (RS). The base materials are securely clamped with the help of manual top clamps. Researchers suggested that the low-quality metal should be put on RS. The parent metal with higher hardness, tensile strength, yield strength, and percentage of elongation is usually placed on the AS. The friction produced on the AS is significantly higher and so is the heat generated. The additional heat produced aids in the plasticization of the harder material placed on the advancing side [34–37]. The photographic view of materials to be welded located in the FSW setup is depicted in Figure 2(b). Figure 3 displays the photographic image of before and after friction stir-welded copper and steel plates.

The machine spindle is spinning at a particular speed and the tool is plunged between the two plates for 3 mm. The tool rotates up to 15 s to dwell at the starting point of the specimen to generate heat for the material. Figure 3(b) shows the sample welded using the FSW process. The rotating spindle initially moves and stirs the material starting from positive Y direction to negative Y direction and thus revolving clockwise. The welding process takes place between the two workpieces. The starting of the workpieces was joined

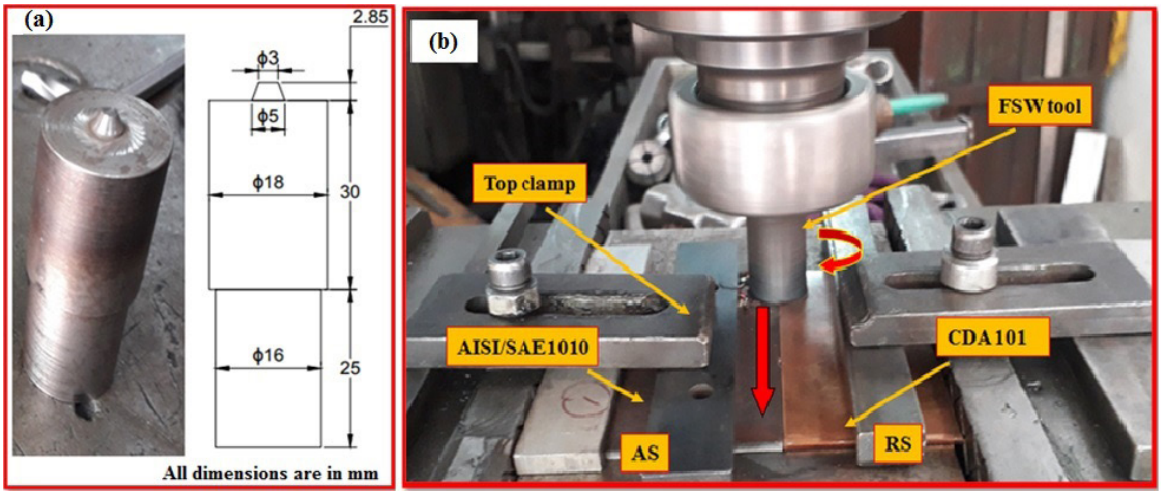

Figure 2. (a) Tapered pin profiled tool. (b) The FSW process and material arrangement setup.

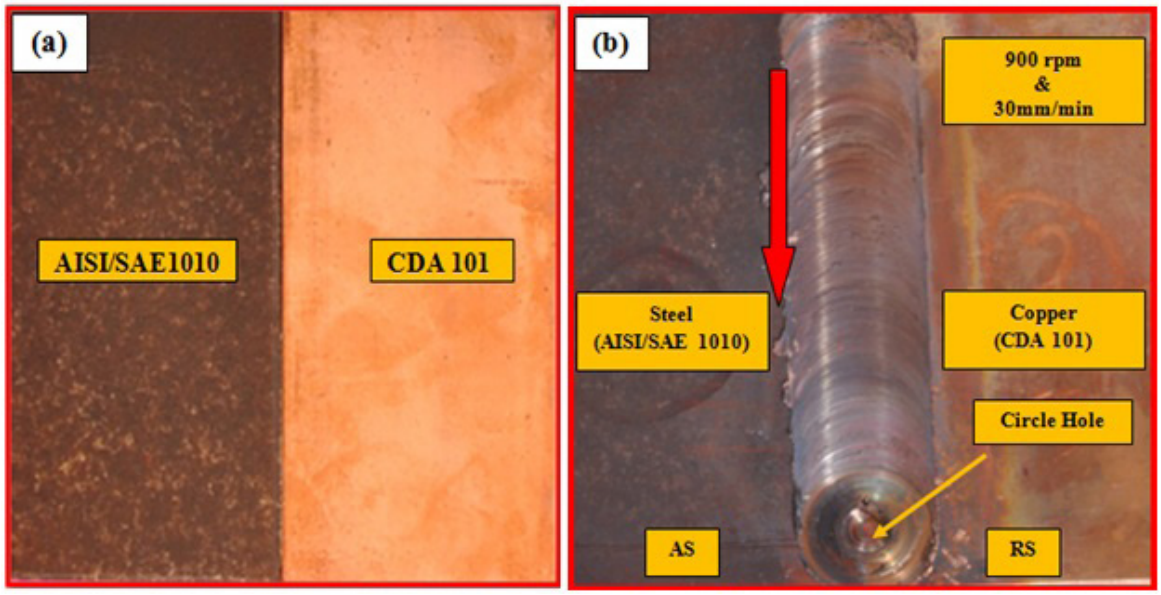

Figure 3. Before and after welding copper and steel plates. (a) Before welding; (b) After welding.

(welded) along −Y direction for 85 mm. At the end point of the joining process, the FSW tool led to stay for 15 s before being extracted at the revolving condition. At the end of the welding operation, the additional welding splash was removed by the grinding process. Mechanical properties depended on the impact of the tool pin profile. The different friction stir tools were used to join Al alloys. A taper threaded pin was used to enhance the tensile and flexure strength [38]. The welding speed, rotational speed, tool geometry, axial force, and its effects were investigated. Mechanical friction has produced the heat on the workpiece with the help of a rotating tool [39].

The sliced specimens are polished by a fine mixture of flaky powder and water and these mixtures were spread over a soft cloth on the rotating disc. The test samples are thoroughly washed and cleaned by water, 5% nitric acid, and ethanol for copper and LCS plates. The microstructure of the weld samples was obtained by using optical microscopy (OM) (De-winter material plus version 2 software, 12V, 50 W halogen lamp) and scanning electron microscopy (SEM) techniques. The plates were cleaned electrolytically in the cross-zone with 10% perchloric acid and 90% alcohol at 25 V and −35°C. The composition was analysed using an electron dispersive spectrometer (EDS). The microhardness experiment was conducted on the transverse zone of the joint using a micro Vickers hardness tester (Wilson Wolpert model). The microhardness testing was conducted at a load of 100 g and a dwell time of 10 s. Uniform distance (0.5 mm) was maintained to conduct a hardness test on the surface of the welding direction. The microhardness reading is plotted in a graph to understand the hardness at the various welding zone.

The tensile test was carried out as per the ASTM: E8-04 standard with a travel speed of 1.5 mm/min [40]. The tensile sample was prepared as per the dimension of 100 mm × 50 mm × 3 mm in the welding track as shown in Figure 4. The tensile test was conducted at room temperature using the INSTRON 8801 testing machine. The fracture surface of the tensile samples has been analysed by using SEM (JSM 6700F).

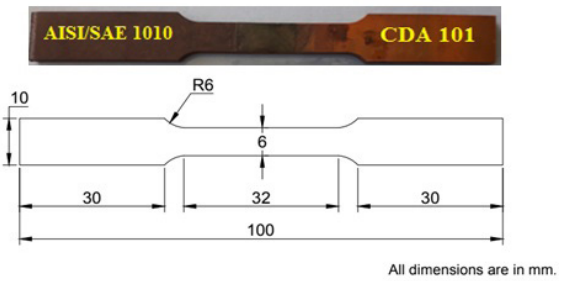

Figure 4. Dimensions [ASTM E8-04] of the tensile sample.

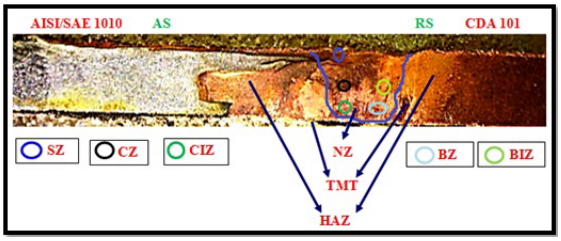

Figure 5. The macropattern of the weld joint b/w copper and LCS.

3. Results Analysis and Discussion

3.1. Macrostructure analysis

Figure 5 depicts the macrostructure of the defect-free weld specimen in various zones. It was carried out by the optical trinocular microscope. The FSW tool revolving speed and the welding speed are very crucial factors. Because both dissimilar materials are mixed and the properties of the mixed zone are dependent on these parameters. From Figure 5, it was clearly indicated that there are no defects identified in the welded samples. To achieve a good microstructure with fine grains and mechanical properties, the material flow is important [37].

The gap between the two plates is very important since it decides the soundness of the welding quality in the FSW operation. Figure 5 depicts the appearance of the weld surface and it is evident that the weld is of good quality. Also, no holes or cracks are observed on the surface which is due to the absence of distortion during welding. The material is spreading outside of the welding zone while increasing the travel speed. Concavity is possible in the FSW process due to the impact of the tool on the workpiece and thus plastic deformation during joining [41].

Figure 5 shows the blend zone of FSW joints of Copper grade CDA 101 and LCS AISI/SAE grade 1010 plates. This zone seems to be dull and light zones when this zone subjected to Keller reagent. This is due to the different levels of degree of material flow during stir processing. Nugget zone (NZ) is seen at the centre of the joint which evident the plastic flow of material from AS (LCS AISI/SAE grade 1010 plates) to the RS (Copper grade CDA 101). The mechanical mixing of materials is achieved due to the advancing of the tool. The joint is identified as defect less one after making an observation in various zones as shown in Figure 5 such as the HAZ on the AS, the HAZ on the RS, the TMT on the (AS-TMT), the TMT on the (RS-TMT), the NZ. In the interim, on the head of material flow portrayal in the NZ, five zones can be other than that distributed with different zones in Figure 5: (1) shoulder zone (SZ), (2) centre zone (CZ), (3) centre interface zone (CIZ), (4) bottom interface zone (BIZ), and (5) bottom zone (BZ). The root defects of the welded joints have been eliminated due to sufficient dynamic recrystallization. The microstructure analysis and mechanical behaviours of the welded joints have been investigated in FSW of Al alloy [42].

3.2. Microstructure analysis

Figure 6(a–b) shows the microstructure of parent materials copper and steel, respectively. In parent materials, the grains are arranged perfectly due to the cold working and plastic deformation. Figure 6(c) shows the microstructure of HAZ and Figure 6(d) shows the TMT. Figure 6(e) shows the interface zone and Figure 6(f) shows the nugget of the joint. The equal size of refined grains of base materials is shown in Figure 6(a–b). This is due to the effect of using an LCS

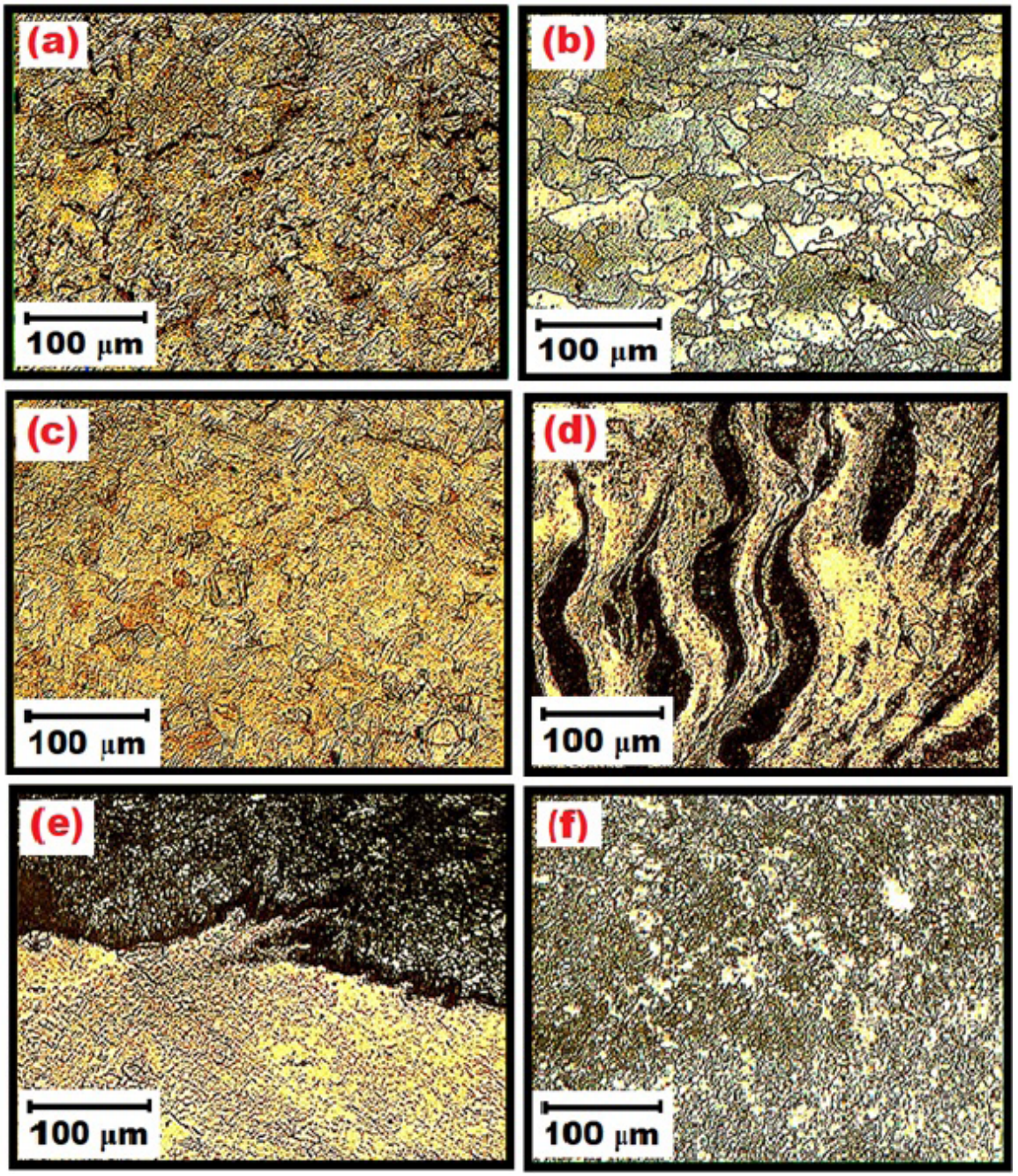

Figure 6. Microstructure of FSW joint of copper and LCS: (a) Cu–parent, (b) steel–parent, (c) Cu HAZ, (d) Cu TMT, (e) Cu–interface, and (f) Nugget.

tool for the FSW process [43–45]. The dynamic rearrangement of particles is responsible for the development of uniform grains in FSW. These grains are developed due to the (i) DDRX (Discontinuous Dynamic Recrystallization), for instance, standard recrystallization which works by nucleation and grain improvement; (ii) CDRX (Continuous Dynamic Recrystallization), which joins the ability in little edge limits into high edge cutoff centres, and (iii) TDRX (Twinning-Induced Dynamic Rearrangement, made by irregularity of the secured grains [46]. Figure 6(c) shows the microstructure of the HAZ and it seems to be similar to the microstructure of parent materials. However, the slight coarsening observed in this zone is because of the transmission of heat from the NZ.

Figure 6(d–e) shows the microstructure of the thermomechanical zone. The image shows that these surfaces are affected by the tool face and tool pull and push. The materials experiencing twisting and deformation between two dissimilar materials. The material in the TMT experiences minimum temperature and deformation. This ensures the absence of recrystallization in this zone.

Figure 6(f) shows the NZ of the joint and it clearly displays that the materials bonded well together because of plastic deformation. The uniform grains observed in this zone are due to the strong plastic shearing and significant heat treatment [47]. The mechanical properties have been changed with respect to the macrostructure and microstructure of the welded joints. The failure mode of fracture has been identified in the NZ and HAZ of the welded joints [48].

3.3. SEM analysis

Figure 7(a) shows the SEM micrograph of parent materials (steel). The microstructure shows extended grains of pearlite in the ferrite of the steel plate. The grain size is assessed as 45 microns. Figure 7(b) shows the parent metal copper with fine-equiaxed grains and with explicit regions of twinning shows up as equal lines. Figure 7(c) depicts the microstructure

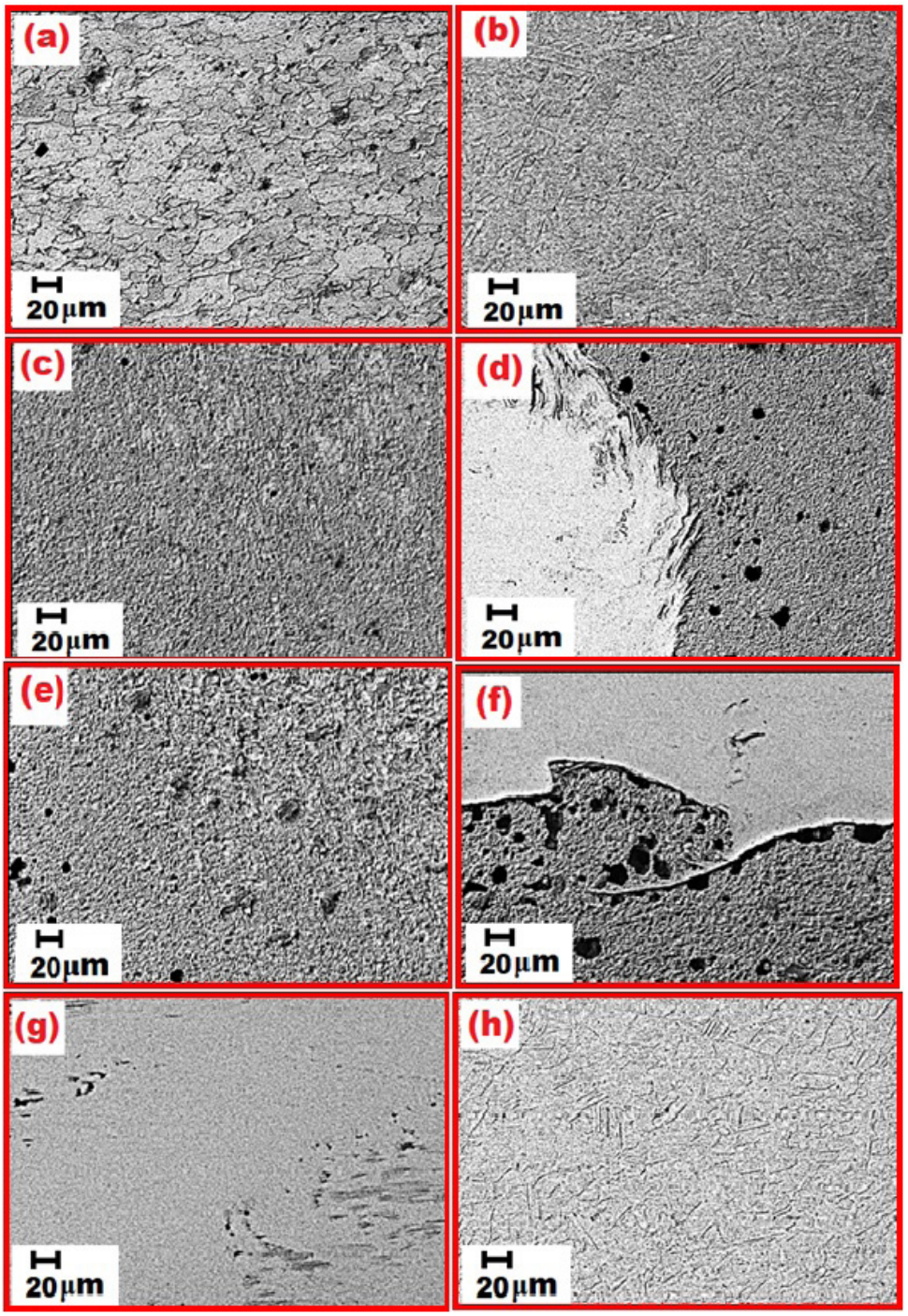

Figure 7. SEM microstructure of FSW joint of copper and LCSs; (a) parent steel, (b) Cu–parent, (c) steel nugget, (d) Cu–St nugget, (e) interface St–Cu, (f) St–Cu bottom, (g) Cu–shoulder, and (h) Cu–HAZ.

of the stir zone of steel. The enhancement is evident that the irregularity and recrystallization have occurred and the grain sizes are in the solicitation for 10 microns. The vertical interface zone of the FSW strategy in the welding zone of copper and steel is shown in Figure 7(d). The steel structure at the right side shows the effect of the stir process with frictional heat incited the crack of grains. The copper at the left side experienced significant plastic flow and the mixed zone is persuading. In Figure 7(e), SEM micrograph shows two microstructures. The right side shows the HAZ and the left half of the picture shows the mechanically affected zone. NZ evident the uniform starring of both the materials and this is due to the plastic deformation during FSW [49]. Figure 7(f) shows the bottom interface zone of copper and steel. The bottom of the picture shows the heat-affected microstructure of the steel and the top shows the piece zone of the copper structure. The copper grains are better and could not be settled. The micrograph shows extensive flexibility of copper metal and the interface zone shows the mix of two metals. The copper network close to the piece zone and the metal system experienced genuine flexibility and grains are fine in all likelihood due to dynamic crystallization showed up in Figure 7(g). The micrograph shows the broad adaptability of copper metal and the interface zone shows the blend of two metals. The copper network near the piece zone and the metal framework experienced absolute malleability and grains are fine more than likely because of dynamic crystallization that appeared in Figure 7(g). Figure 7(h) shows the HAZ of the FSW process at the copper side. The grain size of copper is seen as higher. The austenitic structure was produced due to dynamic recrystallization under different welding speeds. The excellence of the welded joints without defects was attained at a welding speed of 30–70 mm/min [50-51].

3.4. EDAX analysis

Figure 8(a–c) shows the EDAX results of friction stir welded samples. Figure 8(a) shows the results of the EDS analysis done on the copper side. Some oxides are found in the graph which evident the heat-affected in these zones during stirring. Hence the parent materials with some oxides

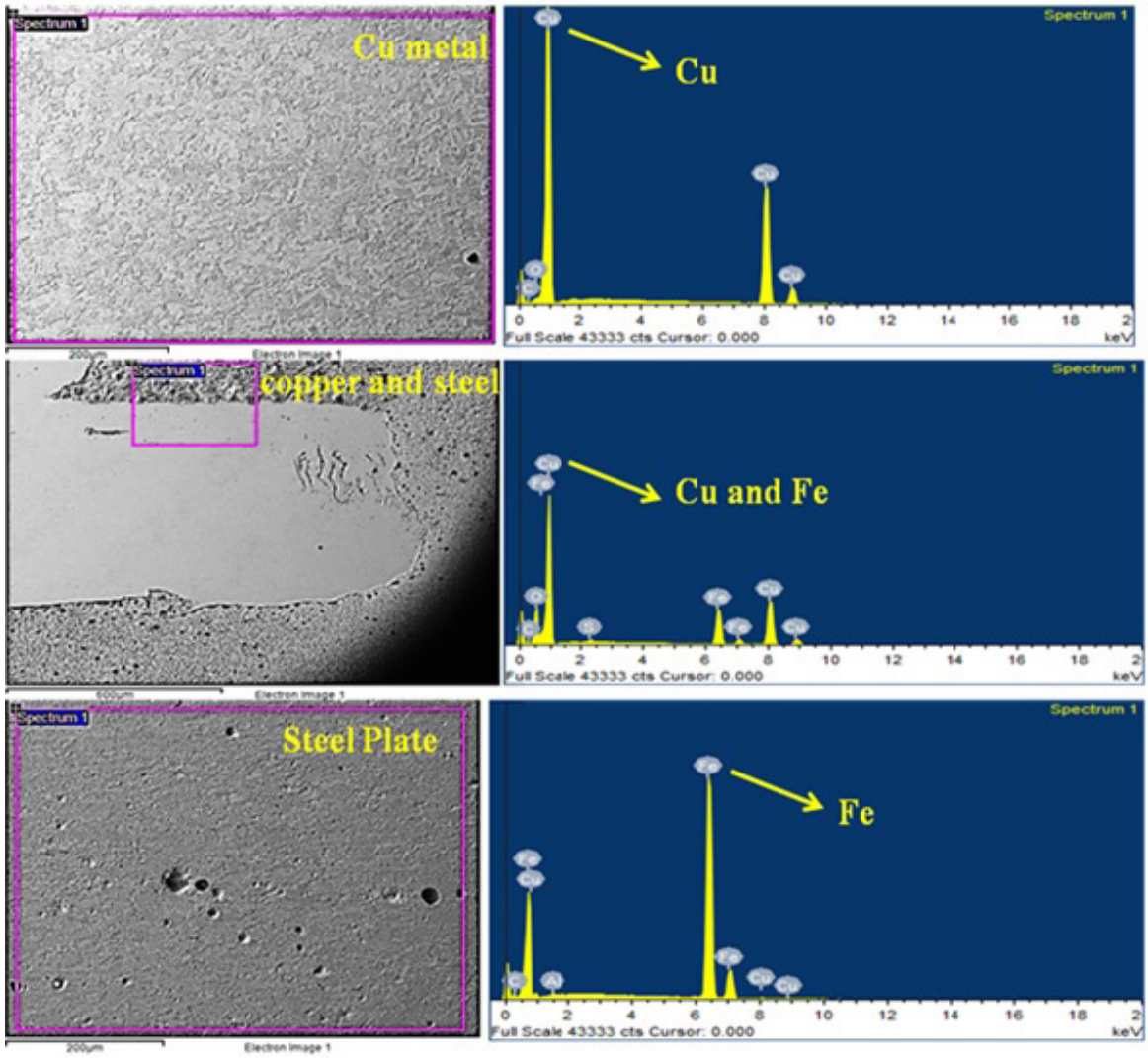

Figure 8. Elemental analysis of copper and steel at the NZ.

are observed. Figure 8(b) shows the EDAX results taken at the interface weld zone. It ensures both steel and copper elements in this zone. From the SEM image, it is obvious that the interfacing between copper and steel is good. In this EDAX graph, two rich elements are observed such as Fe and Cu. In addition, the presence of oxygen ensures the formation of oxides during welding. Figure 8(c) shows the EDAX graph obtained from the steel side of the welded joint. The presence of Fe ensures the other side of the steel plate. The study revealed that copper and steel is mixed well enough to make defect-free joint [52].

3.5. Mechanical behaviours

3.5.1. Microhardness distribution

Figure 9 shows graphical representation of the higest hardness obatined for the welded sample. The lowest hardness is observed in the HAZ. The hardness value increases in the thermomechanical-affected zone. The highest hardness is observed in the NZ when compared with the HAZ and TMT. The hardness is lower at the outer surface of the NZ. The hardness is higher in the weld zone when compared with parent materials. It is esteemed that the hardness is reliably impacted by grain size as showed up with Hall–Petch condition [53-54]. The improved hardness is due to the grain refinement during stirring action. Fine equiaxed grains acquired in NZ occurred thus the most tremendous microhardness is reached. The welding is carried out at a speed of 30 mm/min, which created dynamic recrystallization at the NZ. The lowest hardness at HAZ is due to the coarse grain structure at the outer surface of the weld zone [55]. Travel speed was the most influential actors in mechanical properties. Initially, the ultimate tensile strength has been increased with the increase of traverse speed, and then it has been decreased due to the formation of defects [56].

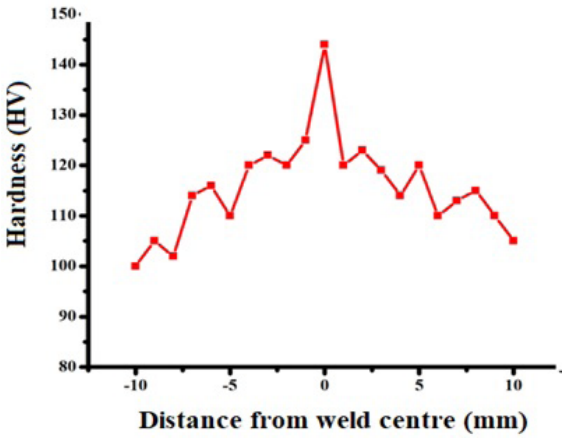

Figure 9. Microhardness distribution dissimilar weld joint b/w copper and LCS.

3.5.2. Tensile behaviour and fracture morphology

Figure 10(a) shows the tensile samples made using at 900 rpm and 30 mm/min after the tensile test. The sample shows defect-free joint welded LCS AISI/SAE grade 1010 with copper grade CDA 101. It is noted that in all weld samples the fracture occurred at the mid-portion of weld nugget at the stirred zone. This is because of the execution of uniform material flow and grain alignment. The uniform distribution of stress in the stir zone finely transfer the applied load throughout the weld nugget thus the fracture occurred at the middle. Moreover, the fractured portion shows cup and cone fracture, which indicates the ductile nature of the weld bead. This is because of retained ductility in the stir zone by the implication of optimized input process parameters. The fine mixture of both copper and iron atoms still retains the ductility in the weld nugget. However, the formation of cup and cone is marginally less due to the increased brittleness by the high speed stirred zone. The highly stirred parent metals and quick solidification was the cause of greater brittleness. The mechanical properties of welded joint are presented in Table 2. The tensile strength of 181.5 MPa is obtained at the NZ. The elongation of 14.03% is obtained for the welded sample. Figure 10(b) and (c) shows fracture SEM images of the welded sample. The fractography is at 500X which has shown both the matrix of copper and steel. The copper matrix grains show higher plasticity with grain flow. The fractured region with copper and fusion zone shows the plastic flow of the ductile matrix of copper with the orientation of the grains. The fusion zone shows the transition region of both the metals. The fusion zone shows no void and the copper at the fusion zone shows the dense flow of grains by fracture. Both the parent materials are perfectly stirred in the NZ, which we conclude that is the material fracture behaviour gained like a brittle fracture mode. Because the tool spinning speed (spindle speed) is majorly influenced to create frictional heat between both the materials during the joining process at the end of the stage good sound weld joints are obtained. The perfect material flow (plasticized range) is the homogeneous and equiaxed size of grain particles that were measured after done by the fractography test for broken specimens. The entire fracture structure gained dimple mode. The tensile fracture surface of the copper morphology is finer and is evident to show a higher elongation. The fusion zone is at the centre and the

Table 2. Mechanical properties of the welded joint.

S.no.	Tensile strength (MPa)	Hardness VHN	% of elongation	Max.strain
1	181.5	144	14.03	35.83
2.	176.3	139	13.59	25.68
3.	167.5	136	12.98	23.5
4.	169.89	129	12.03	24.79
5.	170.4	131	12.54	25.98

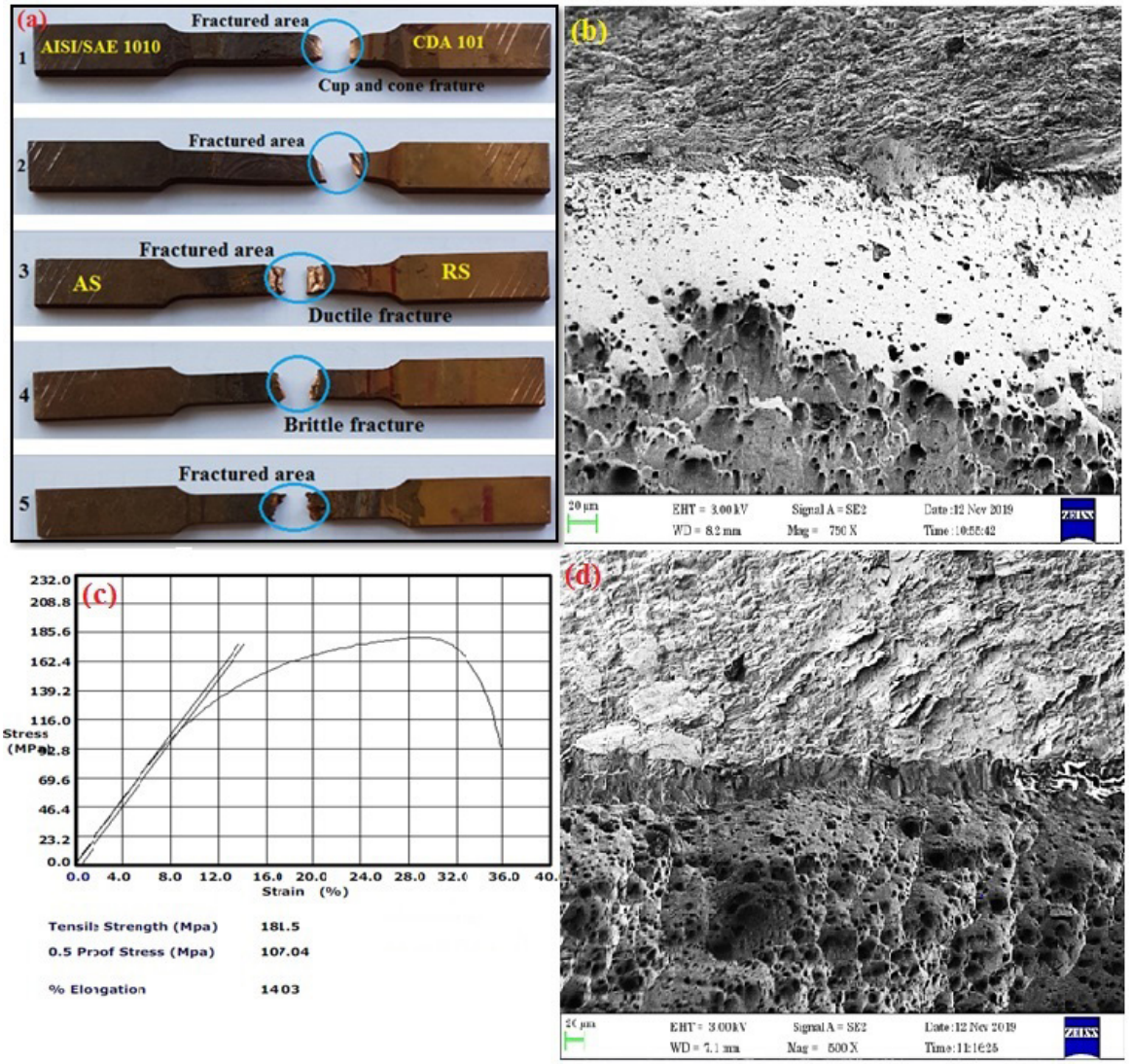

Figure 10. Tensile measurements: (a) fracture locations of the joint, (b,c) tensile rupture features of the weld joint, and (d) stress–strain curv e for fractured specimen.

fusion is complete without any void or separation during the fracture. The residual stresses and fracture defects were investigated in FSW of dissimilar welded joints. The greatest tensile strength (170 MPa) of the joints were produced when the tool rotation of 1000 rpm and its traverse speed of 150 mm/min [57-58].

The copper grains show higher adaptability with grain flow and the steel sort out shows no flow of grains [59]. The interface junction at the NZ shows the fusion of the copper and the steel. The bottom zone is a copper matrix and the top is the steel matrix. At the fusion, the line is enriched with copper metal. The steel zone shows fine fragmented grains of pearlite in the ferrite matrix with typical LCS. The copper side has undergone severe plasticity and the effect is observed with a substantial flow of copper metal. The grains of steel are very fine for the order of 5 microns. Figure 10(d) indicates the stress–strain curve for the fractured tensile specimen in a spindle revolving rate of 900 rpm and a travelling speed of 30 mm/min.

3.5.3. Examination of Force Generation analysis

FSW process applied three different forces to the base material: transverse force, longitudinal force, and axial force in the X, Y, and Z axes, respectively. Figure 11 shows the welding force generated by constant FSW process parameters such as 900 rpm rotation speed, 30 mm/min welding speed, and 5 KN constant axial load. Adjusting process parameters has a direct effect on the frictional force generated during the fabrication of FSW joints. The downward force achieved its maximum value when the tool was sinking between the materials to be joined and the shoulder reached the material's surface [60]. Two peak values for the downward force were obtained at a rotating speed of 900 rpm; 4.3 kN for the force acting on the pin when sinking into the parent material, and

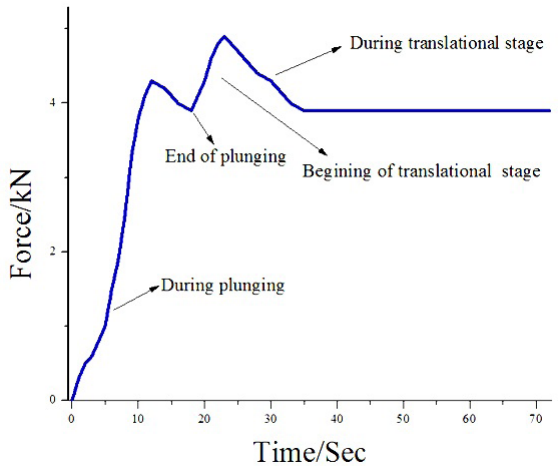

Figure 11. Axial force generation during FSW process.

4.9 kN for the force acting on the shoulder contact with the base material. The force dropped substantially during the transnational stage, maintaining at 3.9 kN until the tool was withdrawn from the material. The force dropped considerably during the transnational stage and remained constant at 3.9 kN until the tool was withdrawn from the material after the joining process. The primary source of downward force was the tool shoulder. Its downward force increased as welding speed increased. This could be because the materials thermal softening has decreased. The downward force decreases as the tool's rotational speed increased [61]. This might be because as the rotational speed increased, the material's temperature increased, causing it to become thermally softened and plasticized more quickly.

4. Conclusions

In this study, copper grade CDA 101 and LCS AISI/SAE grade 1010 samples were successfully welded using FSW at a tool rotational speed of 900 rpm and welding speed of 30 mm/min. Also, the morphology and mechanical behaviours of the joints were fruitfully investigated. Based on this experimental study, the following conclusions were drawn.

- The fine equiaxed grain structure was observed by using SEM and OM at the NZ for the samples welded at 30 mm/min.
- From the SEM analysis, it is found that the steel structure at the right side shows the impact of the mixing process with frictional heat actuated the split of grains. The left side copper experienced significant plastic flow and the interface mix zone is identified.
- The tensile strength of 181.5 MPa along with the elongations is 14.03% obtained for the welded samples. The sheer zone and NZ were distinguished at the tensile specimen crack surface which demonstrated a run of the typical ductile fracture.
- In this experimental analysis, it was identified that the employment of FSW technique can produce a weld joint with nearly 80–85% of the actual strength of the parent metal. This is a high value when compared with other joining techniques.
- Based on the current findings, a few areas of future research have been identified, such as adding metallic or ceramic fillers into the welding zone to improve the strength and quality of the weld bead and optimizing the fillers content for the best desirable outcomes in the weldments.
- This study has paved a pathway for joining of dissimilar metals like copper grade CDA 101/ AISI-SAE1010 grade low carbon steel. In addition to this experimental investigation, this approach of friction stir welding opens up a wider range of possibilities for joining a variety of different metals such as titanium, brass, etc.

5. References

1. Jahanzeb N, Shin JH, Singh J, Heo YU, Choi SH. Effect of microstructure on the hardness heterogeneity of dissimilar metal joints between 316L stainless steel and SS400 steel. Mater Sci Eng A. 2007;700:338-50.
2. Fu B, Qin G, Li F, Meng X, Zhang J, Wu C. Friction stir welding process of dissimilar metals of 6061-T6 aluminum alloy to AZ31B magnesium alloy. J Mater Process Technol. 2015;218:38-47.
3. Jafarzadegan M, Abdollah-Zadeh A, Feng AH, Saeid T, Shen J, Assadi H. Microstructure and mechanical properties of a dissimilar friction stir weld between austenitic stainless steel and low carbon steel. J Mater Sci Technol. 2003;29:367-72.
4. Babu SDD, Sevvel P, Senthil Kumar R, Vijayan V, Subramani J. Development of thermo mechanical model for prediction of temperature diffusion in different FSW tool pin geometries during joining of AZ80A Mg alloys. J Inorg Organomet Polym Mater. 2021;31:3196-212.
5. Mostaan H, Safari M, Bakhtiari A. Micro friction stir lap welding of AISI 430 ferritic stainless steel: a study on the mechanical properties, microstructure, texture and magnetic properties. Metallurgical Research and Technology. 2018;115:307.
6. Satheesh C, Sevvel P, Kumar RS. Experimental identification of optimized process parameters for FSW of AZ91C Mg alloy using quadratic regression models. J Mech Eng. 2020;66(12):736-51.
7. Badheka VJ, Basu R, Omale J, Szpunar J. Microstructural aspects of TIG and ATIG welding process of dissimilar steel grades and correlation to mechanical behavior. Trans Indian Inst Met. 2016;69:1765-73.
8. Esfahani MN, Coupland J, Marimuthu S. Microstructure and mechanical properties of a laser welded low carbon-stainless steel joint. J Mater Process Technol. 2014;214:2941-8.
9. Simar A, Avettand-Fènoël M-N. State of the art about dissimilar metal friction stir welding. Sci Technol Weld Join. 2017;22(5):389-403.
10. Magalhães VM, Leitão C, Rodrigues DM. Friction stir welding industrialisation and research status. Sci Technol Weld Join. 2018;23(5):400-9.
11. Mira-Aguiar T, Verdera D, Leitão C, Rodrigues DM. Tool assisted friction welding: a FSW related technique for the linear lap welding of very thin steel plates. J Mater Process Technol. 2016;238:73-80.
12. Giridharan K, Sevvel P, Gurijala C, Yokesh Kumar B. Biochar-assisted copper-steel dissimilar friction stir welding: mechanical, fatigue, and microstructure properties. Biomass Conv Bioref. 2021:1-11.
13. Benghalia G, Rahimi S, Wood J, Coules H, Paddea S. Multiscale measurements of residual stress in a low alloy carbon steel

weld clad with IN625 superalloy. Materials Performance and Characterization. 2018;7:606-29.
14. Easton D, Wood J, Rahimi S, Galloway A, Zhang Y, Hardie C. Residual stress generation in brazed tungsten dissimilar joints. IEEE Trans Plasma Sci. 2016;44:1625-30.
15. Sevvel P, Babu SDD, Kumar RS. Peak temperature correlation and temperature distribution during joining of AZ80A Mg Alloy by FSW – a numerical and experimental investigation. J Mech Eng. 2020;66(6):395-407.
16. Padhy G, Wu C, Gao S. Friction stir based welding and processing technologiesprocesses, parameters, microstructures and applications: a review. J Mater Sci Technol. 2018;34:1-38.
17. Kayode O, Akinlabi ET. An overview on joining of aluminium and magnesium alloys using friction stir welding (FSW) for automotive lightweight applications. Mater Res Express. 2019;6:112005.
18. Sevvel P, Satheesh C, Senthil Kumar R. Generation of regression models and multi-response optimization of friction stir welding technique parameters during the fabrication of AZ80A Mg alloy joints. Trans Can Soc Mech Eng. 2020;44:311-24.
19. Zhang X, Chen Y, Hu J. Recent advances in the development of aerospace materials. Prog Aerosp Sci. 2018;97:22-34.
20. Azarniya A, Taheri AK, Taheri KK. Recent advances in ageing of 7xxx series aluminum alloys: a physical metallurgy perspective. J Alloys Compd. 2019;781:945-83.
21. Giridharan K, Sevvel P, Senthilnathan K, Muthukumaran S, Padmanabhan S. Experimental study on mechanical properties of friction stir welded dissimilar joints of aluminium alloys AA8011-AA6082. International Journal of Vehicle Structures and Systems. 2019;11:135-9.
22. Zhang C, Huang G, Cao Y, Zhu Y, Liu Q. On the microstructure and mechanical properties of similar and dissimilar AA7075 and AA2024 friction stir welding joints: effect of rotational speed. J Manuf Process. 2019;37:470-87.
23. Liu ZL, Ji SD, Meng XC. Joining of magnesium and aluminum alloys via ultrasonic assisted friction stir welding at low temperature. Int J Adv Manuf Technol. 2018;97:4127-36.
24. Khodadadi A, Shamanian M, Karimzadeh F. Microstructure and mechanical properties of dissimilar friction stir spot welding between St37 steel and 304 stainless steel. J Mater Eng Perform. 2017;26:2847-58.
25. Matlan MJB, Mohebbi H, Pedapati SR, Awang MB, Ismail MC, Kakooei S, et al. Dissimilar friction stir welding of carbon steel and stainless steel: some observation on microstructural evolution and stress corrosion cracking performance. Trans Indian Inst Met. 2018;71:2553-64.
26. Jafarzadegan M, Feng AH, Abdollah-Zadeh A, Saeid T, Shen J, Assadi H. Microstructural characterization in dissimilar friction stir welding between 304 stainless steel and st37 steel. Mater Charact. 2012;74:28-41.
27. Sevvel P, Satheesh C. Role of tool rotational speed in influencing microstructural evolution, residual-stress formation and tensile properties of friction-stir welded AZ80A Mg alloy. Mater Technol. 2018;52:607-14.
28. Rahimi S, Konkova T, Violatos I, Baker TN. Evolution of microstructure and crystallographic texture during dissimilar friction stir welding of duplex stainless steel to low-alloy structural steel. Metall Mater Trans, A Phys Metall Mater Sci. 2019;50:644-87.
29. Fujii H, Cui L, Tsuji N, Maeda M, Nakata K. Friction stir welding of carbon steels. Mater Sci Eng A. 2006;429(1):50-7.
30. Thomas WM, Threadgill PL, Nicholas ED. Feasibility of friction stir welding steel. Sci Technol Weld Join. 1999;4(6):365-72.
31. Lienert TJ, Stellwag WL, Grimmett BB, Warke RW. Friction stir welding studies on mild steel: process results, microstructures, and mechanical properties are reported. Weld J. 2003;82(1):1S-9S.
32. Karami S, Jafarian H, Eivani AR, Kheirandish S. Engineering tensile properties by controlling welding parameters and microstructure in a mild steel processed by friction stir welding. Mater Sci Eng A. 2016;670:68-74.
33. Ghosh M, Hussain M, Kumar GR. Effect of welding parameters on microstructure and mechanical properties of friction stir welded plain carbon steel. ISIJ Int. 2012;52(3):477-82.
34. Micallef D, Camilleri D, Toumpis A, Galloway A, Arbaoui L. Local heat generation and material flow in friction stir welding of mild steel assemblies. Proceedings of the Institution of Mechanical Engineers, Part L. 2016;230(2):586-602.
35. Thangaiah ISS, Sevvel P, Satheesh C, Jaiganesh V. Investigation on the Impingement ofParameters of FSW Process on the Microstructural Evolution & Mechanical Properties of AZ80A Mg Alloy Joints. FME Transactions. 2018;46:23-32.
36. Fernandez JR, Ramirez AJ. Microstructural evolution during friction stir welding of mild steel and Ni-based alloy 625. Metall Mater Trans, A Phys Metall Mater Sci. 2017;48:1092-102.
37. Sevvel P, Satheesh C, Jaiganesh V. Influence of tool rotational speed on microstructural characteristics of dissimilar Mg alloys during friction stir welding. Trans Can Soc Mech Eng. 2019;43:132-41.
38. Gupta MK. Effects of tool profile on mechanical properties of aluminium alloy Al 1120 friction stir welds. J Adhes Sci Technol. 2020;34(18):2000-10.
39. Rajak DK, Pagar DD, Menezes PL, Eyvazian A. Friction-based welding processes: friction welding and friction stir welding. J Adhes Sci Technol. 2020;34:2613-37.
40. Sevvel P, Jaiganesh V. Investigation on evolution of microstructures and characterization during FSW of AZ80A Mg alloy. Arch Metall Mater. 2017;62:1779-85.
41. Su JQ, Nelson TW, Mishra R, Mahoney M. Microstructural investigation of friction stir welded 7050-T651 aluminium. Acta Mater. 2003;51:713-29.
42. Huang G, Cheng D, Wang H, Zhou Q, Shen Y. Effect of tool probe with a disc at the top on the microstructure and mechanical properties of FSW joints for 6061-T6 aluminum alloy. J Adhes Sci Technol. 2019;33(22):2462-75.
43. Jata KV, Semiatin SL. Continuous dynamic recrystallization during friction stir welding of high strength aluminum alloys. Scr Mater. 2000;43:743-9.
44. Cho J-H, Jae Kim W, Gil Lee C. Texture and microstructure evolution and mechanical properties during friction stir welding of extruded aluminum billets. Mater Sci Eng. 2014;597:314-23.
45. Bayazid SM, Farhangi H, Asgharzadeh H, Radan L, Ghahramani A, Mirhaji A. Effect of cyclic solution treatment on microstructure and mechanical properties of friction stir welded 7075 Al alloy. Mater Sci Eng. 2016;649:293-300.
46. Sevvel P, Jaiganesh V. Influence of the arrangement of materials and microstructural analysis during FSW of AZ80A & AZ91C Mg alloys. Arch Metall Mater. 2017;62:1795-801.
47. Shojaei K, Sajadifar SV, Yapici GG. On the mechanical behavior of cold deformed aluminum 7075 alloy at elevated temperatures. Mater Sci Eng. 2016;670:81-9.
48. Guo C, Shen Y, Hou W, Yan Y, Huang G, Liu W. Effect of groove depth and plunge depth on microstructure and mechanical properties of friction stir butt welded AA6061-T6. J Adhes Sci Technol. 2018;32(24):2709-26.
49. Ekinci O, Balalan Z. Effect of tool pin geometry on microstructure and mechanical properties of friction stir spot welds of 7075-T651 aluminium alloy. Metall. 2021;118(1):110.
50. Teker T, Karakurt EM, Özabaci M, Güleryüz Y. Investigation of the weldability of AISI304 and AISI1030 steels welded by friction welding. Mettallurigical Research and Technology. 2020;117(6):601.
51. Guo R, Shen Y, Huang G, Zhang W, Guan W. Microstructures and mechanical properties of thin 304 stainless steel sheets by friction stir welding. J Adhes Sci Technol. 2018;32(12):1313-23.
52. Sevvel P, Jaiganesh V. Effect of tool shoulder diameter to plate thickness ratio on mechanical properties and nugget zone

characteristics during FSW of dissimilar Mg alloys. Trans Indian Inst Met. 2015;68(S1):41-6.
53. Viscusi A, Astarita A, Prisco U. Mechanical Properties optimization of friction stir welded lap joints in Al alloy. Adv Mater Sci Eng. 2016;201(9):3832873.
54. Kumar RA, Muneeswaran R, Mohan MS, Rengarajan S, Raghav GR, Nagarajan KJ. Effects of tool pin profile on tensile and wear behaviour of friction stir welded AA6101-T6 and AA1350 alloys. Mettallurigical Research and Technology. 2020;117(5):503.
55. Balasubramanian M. Development of processing windows for diffusion bonding of Ti-6Al-4V titanium alloy and 304 stainless steel with silver as intermediate layer. Trans Nonferrous Met Soc China. 2015;25(9):2932-8.
56. Sevvel P, Jaiganesh V. Impact of process parameters during friction stir welding of AZ80A Mg alloy. Sci Technol Weld Join. 2016;21:83-90.
57. Yin K, Cao L, Wang N. Mechanical properties and residual stresses of 5083 to AM60B dissimilar friction stir welding with different process parameters. J Adhes Sci Technol. 2019;33(23):2615-29.
58. Kumar RA, Raghav GR, Nagarajan KJ, Rengarajan S, Suganthi P, Vignesh V. Effect of hybrid reinforcement at stirred zone of dissimilar aluminium alloys during friction stir welding. Mettallurigical Research and Technology. 2019;116(6):631.
59. Sun Q, Di H-S, Wang X-N, Chen X-M, Nie X-K, Chen D-L, et al. Effect of heat input on microstructure and properties of dissimilar laser welded joints between TWIP and TRIP steels. Metall Res Technol. 2019;116(6):616.
60. Krishnan M, Subramaniam SK. Investigation of mechanical and metallurgical properties of friction stir corner welded dissimilar thickness AA5086-AA6061 aluminium alloys. Mater Res. 2018;21(4). http://dx.doi.org/10.1590/1980-5373-MR-2017-1045.
61. Tan CW, Jiang ZG, Li LQ, Chen YB, Chen XY. Microstructural evaluation and mechanical properties of dissimilar Al-CU joints produced by friction stir welding. Mater Des. 2013;51(4):466-73.